J Comp Physiol A (2006) 192: 637–648
DOI 10.1007/s00359-006-0103-z

REVIEW

W. H. Mehaffey · F. R. Fernandez · A. J. Rashid
R. J. Dunn · R. W. Turner

Distribution and function of potassium channels in the electrosensory lateral line lobe of weakly electric apteronotid fish

Received: 18 November 2004 / Revised: 26 October 2005 / Accepted: 26 December 2005 / Published online: 20 January 2006

Abstract Potassium channels are one of the fundamental requirements for the generation of action potentials in the nervous system, and their characteristics shape the output of neurons in response to synaptic input. We review here the distribution and function of a high-threshold potassium channel (Kv3.3) in the electrosensory lateral line lobe of the weakly electric fish *Apteronotus leptorhynchus*, with particular focus on the pyramidal cells in this brain structure. These cells contain both high-threshold Kv3.3 channels, as well as low-threshold potassium channels of unknown molecular identity. Kv3.3 potassium channels regulate burst discharge in pyramidal cells and enable sustained high frequency firing through their ability to reduce an accumulation of low-threshold potassium current.

Keywords Kv3 · Low-threshold K^+ current · Electric fish · Backpropagation · Bursting

Abbreviations CCb: Corpus cerebelli · EGp: Eminentia granularis pars posterior · ELL: Electrosensory lateral line lobe · EOD: Electric organ discharge · GC1: Type-1 granule cells · GC2: Type-2 granule cells · IK_{HT}: High-threshold potassium channel · IK_{LT}: Low-threshold potassium channel · JAR: Jamming avoidance response · LC: Caudal lobe of cerebellum · NADPH-d: Nicotinamide adenine dinucleotide phosphate-diaphorase · TEA: Tetraethylammonium · $V_{1/2}$: Half-activation voltage

W. H. Mehaffey and F. R. Fernandez contributed equally to this work.

W. H. Mehaffey · F. R. Fernandez · R. W. Turner (✉)
Hotchkiss Brain Institute, University of Calgary,
3330 Hospital Dr. N.W., T2N 4N1 Calgary, AB, Canada
E-mail: rwturner@ucalgary.ca
Tel.: +1-403-2208451
Fax: +1-403-2838731

A. J. Rashid
University of Toronto, M5S 1A8 Toronto, ON, Canada

R. J. Dunn
McGill University, H3G 1A4 Montreal, QC, Canada

Introduction

Potassium (K^+) channels are one of the basic requirements for the generation of an action potential (Hodgkin and Huxley 1952). Molecular techniques have defined a large number of families of K^+ channels, each with distinct members, kinetics, voltage dependence, and pharmacology (Chandy and Gutman 1993; Coetzee et al. 1999). Recent work has begun to dissect apart the contribution of kinetically distinct K^+ channel subunits to firing (Shibata et al. 1999; Ishikawa et al. 2003) and to understand the interactions between the subunits themselves (Lee et al. 1996; Baranauskas et al. 2003).

High rates of firing are commonly associated with the expression of high-threshold K^+ currents of the Kv3 family (Rudy and McBain 2001) and are often found in auditory regions requiring high temporal acuity, including areas calculating interaural time delays (Perney et al. 1992; Weiser et al. 1994; Trussell 1997; Gan and Kaczmarek 1998; Wang et al. 1998; Parameshwaran et al. 2001), although their expression has not yet been examined in circuits underlying interaural time delays in electric fish (Carr et al. 1986; Carr and Maler 1986). The computations performed by these highly sensitive midbrain structures require precise timing in their inputs from lower brain regions. Kv3 channels have been shown to be kinetically optimized for high frequency and precisely timed spike output due to their high threshold and fast kinetics (Wang et al. 1998; Lien and Jonas 2003). We can therefore use Kv3 immunolabel as a first approximation to identify high-frequency firing cell types.

The apteronotid weakly electric fish depend on their electrosensory system for many behaviors, including predation (MacIver et al. 2001; Nelson et al. 2002), communication (Zakon et al. 2002; Dunlap and

Larkins-Ford 2003), determining social hierarchy (Dunlap 2002; Dunlap and Oliveri 2002), and the well-studied jamming avoidance response (JAR) (Heiligenberg 1986). The first order structure for processing of electrosensory information is the electrosensory lateral line lobe (ELL), a cerebellum-like structure closely conserved among weakly electric fish. Many wave-type electric fish have high electric organ discharge (EOD) frequencies. *Apteronotus* EOD discharge can be as high as 1,300 Hz, suggesting that temporal information must be encoded with great fidelity. In particular, since some neurons code information about EOD phase, high rates of precisely timed discharge are required. Our recent work has shown significant Kv3 channel expression in electrosensory structures (Rashid et al. 2001a). Moreover, these channels prove to have multiple roles in regulating burst threshold and high-frequency discharge of ELL pyramidal cells (Noonan et al. 2003; Fernandez et al. 2005). This review will focus on the distribution of Kv3.3 channels in the ELL, with particular focus on the separate roles of dendritic and somatic Kv3 currents in ELL pyramidal cell output, and on a newly recognized interaction between Kv3 and low-threshold K^+ currents that allow the high-frequency firing required for accurate transmission of fine details in electrosensory signals.

Distribution of *Apt*Kv3.3 in the apteronotid ELL

Many cells in the ELL of the weakly electric fish *Apteronotus leptorhynchus* express at least one member of the Kv3 family, the apteronotid homolog of the murine Kv3.3b subunit (Rashid and Dunn 1998; Rashid et al. 2001a). We have used a polyclonal antibody developed by our laboratories in order to probe for *Apt*Kv3.3 expression, whose distribution follows that found with in situ mRNA probes (Rashid et al. 2001a). *Apt*Kv3.3 expression can be seen across all maps of the ELL—the medial, centromedial, centrolateral, and lateral segments. The medial segment processes ampullary inputs, while the remaining three maps process tuberous inputs from two types of coding units, T-units and P-units (Heiligenberg 1991). *Apt*Kv3.3 channels are prominently expressed in the ELL pyramidal cell layer, granule cell layer, and deep neuropil layer, and more weakly in the molecular layer (Fig. 1a).

Cells receiving P-unit inputs

Tuberous electrosensory information reaches all three tuberous maps of the ELL through afferents from ganglion cells in the anterior lateral line nerve (Lannoo et al. 1989). Ganglion cell somata, but not the axon hillock or axon, stain positive for *Apt*Kv3.3 (Fig. 1f, g). Pyramidal cells, the primary output neuron of the ELL, as well as the majority of ELL interneurons express the *Apt*Kv3.3 channel. Three separate populations of pyramidal cells can be distinguished—deep, intermediate, and superficial (Bastian and Courtright 1991; Bastian and Nguyenkim 2001; Bastian et al. 2004), all of which label for *Apt*Kv3.3 channels along both the soma and dendrite (Fig. 1b). Figure 1c shows a magnified view to clearly display *Apt*Kv3.3 label in a non-basilar pyramidal cell (Fig. 1c, arrowhead) and the dendrite of a deep pyramidal cell (Fig. 1c, small arrows; deep pyramidal somata can be seen in Fig. 1h, sharp arrowhead). Both type-1 granule cells (GC1) and type-2 granule cells (GC2) express *Apt*Kv3.3 on their somata (Fig. 1d, broad arrowheads—GC1; sharp arrowheads—GC2), but not dendrites (Fig. 1e), as shown by the counterstaining with CaMKII to visualize entire cells. GC1 and GC2 can be distinguished according to dendritic arborizations, since GC2 cells have significant apical arborizations, while GC1 cells do not (Maler 1979). GC2 granule cells inhibit pyramidal cell somata and are the primary input driving non-basilar pyramidal cells (I-units), which code for downstrokes of EOD amplitude modulations. GC1 cells have been suggested to mediate surround inhibition in order to enhance contrast (Maler and Mugnaini 1994). Also expressing *Apt*Kv3.3 channels are polymorphic cells (Fig. 1c, arrow), a class of commissural interneurons that projects to the contralateral ELL where they inhibit GC1 neurons (Bastian et al. 1993; Maler and Mugnaini 1994) to possibly regulate surround inhibition. Multipolar cells are inhibitory neurons in the deep neuropil layer, with bilateral projections that also terminate in this structure (Maler and Mugnaini 1994), and stain positive for *Apt*Kv3.3 (Fig. 1h, broad arrowhead). Interneurons of the ventral molecular layer give rise to inhibitory projections that contact the proximal apical dendrites of pyramidal cells (Maler 1979; Maler et al. 1981; Maler and Mugnaini 1994) and display *Apt*Kv3.3 immunolabel on their somata (Fig. 1i, arrows), dendrites (Fig. 1i, small arrows), and axon hillock (Fig. 1i, arrowheads). These cells have been suggested to produce a novel deterministic mechanism for gain control through dendritic inhibition (Mehaffey et al. 2005), consistent with in vivo results (Bastian 1986a, b). Ovoid cells also stain positive for *Apt*Kv3.3 (Fig. 1j). These cells project contralaterally (Bastian et al. 1993) and give rise to metabotropic $GABA_B$ synapses that provide a prolonged inhibition of basilar dendrites of pyramidal cells (Berman and Maler 1998), inhibiting primary afferent depolarizations.

Cells receiving T-unit inputs

Spherical cells code for precisely phase-locked information about the EOD signal (Heiligenberg 1991) and would be expected to be capable of firing at high frequencies, as do most phase-locked cells in the auditory system (Gan and Kaczmarek 1998). Surprisingly, only a subpopulation of spherical cells are positive for *Apt*Kv3.3 mRNA, suggesting some heterogeneity in their firing properties (not shown). Similar results have been found for N-type calcium channel expression

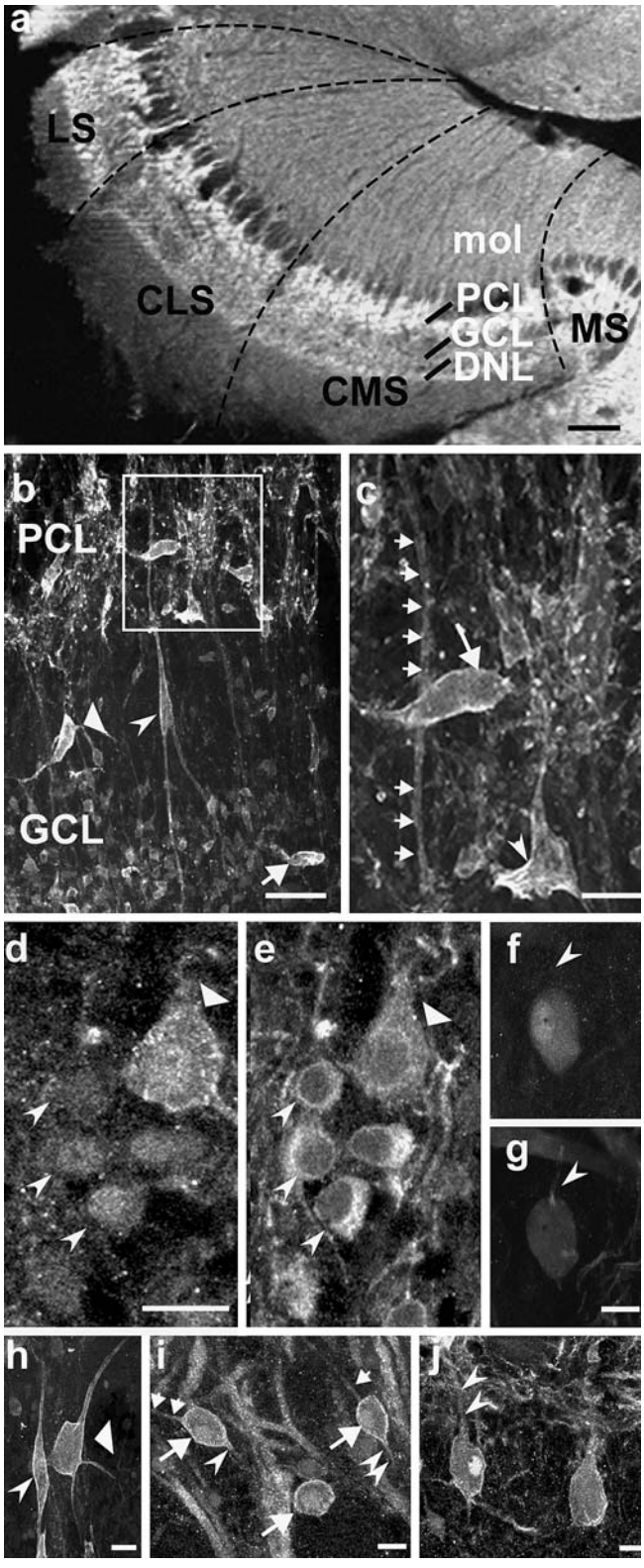

Fig. 1 *Apt*Kv3.3 distribution in the ELL. **a** A low-power image of the ELL indicating the distribution of *Apt*Kv3.3 immunolabel. The boundaries between the four topographic maps (*MS* medial segment, *CMS* centromedial segment, *CLS* centrolateral segment, *LS* lateral segment) are indicated by *dashed lines*. *Apt*Kv3.3 label is found at high density in the pyramidal cell layer (*PCL*), granule cell layer (*GCL*), and deep neuropil layer (*DNL*), and at lower density throughout the molecular layer (*mol*). **b** A low-power image of *Apt*Kv3.3 immunolabeled cells in the PCL, showing a deep basilar pyramidal cell (*arrowhead*), numerous granule cells in the GCL, a multipolar (*broad arrowhead*), and an ovoid cell (*arrow*) in the lateral segment. **c** A magnified view of the area enclosed by a box in **b** includes an *Apt*Kv3.3-labeled polymorphic cell soma (*arrow*), a non-basilar pyramidal cell soma (*arrowhead*), and the apical dendrite of a deep basilar pyramidal cell (*small arrows*). **d, e** A double label for CaMKII (**d**) and *Apt*Kv3.3 (**e**) reveals *Apt*Kv3.3 on the somata of both granule I (*broad arrowhead*) and granule II (*sharp arrowheads*) interneurons in the lateral segment. **f, g** Double labeling for *Apt*Kv3.3 (**f**) and neurofilament protein (**g**) in the anterior lateral line ganglion. *Apt*Kv3.3 immunolabel was found in the cell body of ganglion cells (**f**) but not in the neurofilament-containing primary afferent axons (**g**) that project to the ELL. Note that the axon hillock region is *Apt*Kv3.3 negative (**f**, *arrowhead*). **h** A deep basilar pyramidal cell (*sharp arrowhead*) and multipolar cell (*broad arrowhead*) in the centrolateral segment indicates that cell structure can be delineated by a high density of apparently membrane-associated immunolabel. **i** *Apt*Kv3.3 immunolabels cell bodies in the ventral molecular layer (*arrows*) and their proximal apical dendrites (*small arrows*) in the lateral segment. The proximal segments of cell axons in the ventral molecular layer are denoted by *sharp arrowheads*. Larger diameter pyramidal cell apical dendrites in the region of the tractus stratum fibrosum—ventral molecular layer are nearby. **j** Two ovoid cell bodies located beneath the GCL in the LS. The axonal projection is denoted by *arrowheads*. *Scale bars* 100 μm for **a**, 20 μm for **b**, 10 μm for **c**–**h** and 5 μm for **j**. (Data from Rashid et al. 2001a)

(Tharani et al. 1996) and nicotinamide adenine dinucleotide phosphate-diaphorase (NADPH-d) (Turner and Moroz 1995), supporting the idea that there may be electrophysiologically distinct subtypes of spherical cells. Spherical cells are negative for *Apt*Kv3.3 immunolabel, suggesting that the expression may possibly be limited to the axon or terminal. It is also possible that spherical cells express a different member of the *Apt*Kv3 family.

Although many cell types of the ELL are positive for *Apt*Kv3.3 immunolabel, there are distinct cell types which are negative. Stellate cells, the inhibitory interneurons of the dorsal molecular layer, are not found to be stained nor are the dendrites of the ventral molecular layer or granule cells. Primary afferents projecting from the anterior lateral line lobe, fibers of the tractus stractum fibrosum, and parallel fibers in the molecular layer that project from the granule cells of the eminentia granularis pars posterior (EGp) are uniformly negative.

*Apt*Kv3.3 in the caudal lobe of the cerebellum and the corpus cerebelli

The cerebellum of apteronotid fish, like other teleosts, consists of the corpus cerebelli (CCb), the valvula cerebelli, and the caudal lobe of the cerebellum (LC). This structure rests dorsal to the ELL and contains the EGp. The LC contains an inverted version of the cerebellum with the granule cell layers lying dorsal to the molecular layer (Fig. 2a). The LC provides feedback to the ELL through two systems. The first is the glutamatergic

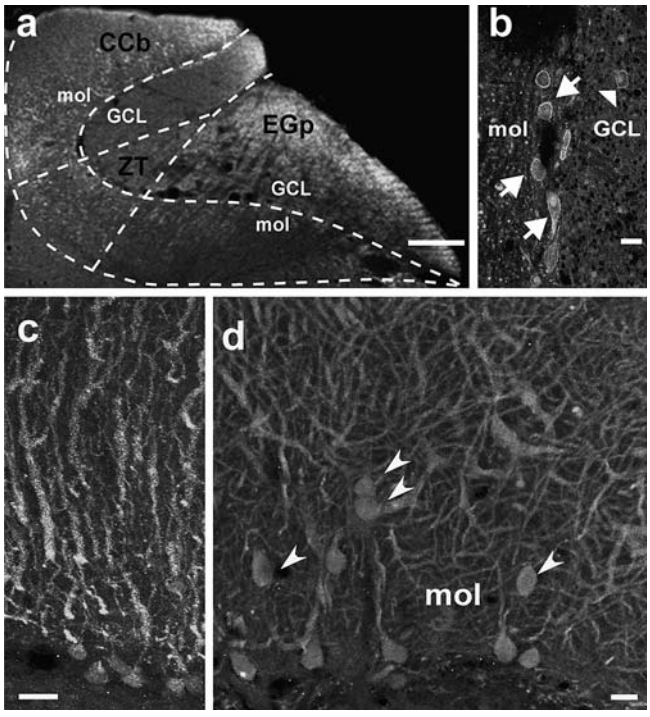

Fig. 2 *Apt*Kv3.3 distribution in the cerebellar lobules. **a** Low-power image of a sagittal section of the cerebellar lobule in the hindbrain, comprised of the corpus cerebelli (*CCb*), a transition zone (*ZT*), and the eminentia granularis pars posterior (*EGp*). *Apt*Kv3.3 immunolabel is of highest intensity in the EGp granule cell layer (*GCL*) and the CCb molecular layer (*mol*). **b** *Apt*Kv3.3 immunolabel in the EGp is localized to eurydendroid cell bodies (*arrows*) positioned at the border of the GCL and molecular layers and putative Golgi cells (*arrowhead*). **c** Putative eurydendroid cell apical dendrites projecting in the EGp molecular layer are positive for *Apt*Kv3.3 immunolabel. **d** CCb, but not EGp, Purkinje cell bodies, and apical dendrites exhibit a high density of *Apt*Kv3.3 label. Purkinje cell bodies scattered through the molecular layer are denoted by *arrowheads*. *Scale bars* 100 μm for **a**, 20 μm for **b**–**d**. (Data from Rashid et al. 2001a)

parallel fibers arising from EGp granule cells (Wang and Maler 1994). The granule cells integrate information from many sources and are not directly excited by pyramidal cells, although they receive electrosensory inputs through multipolar cells of the nucleus praeminentalis dorsalis (Maler et al. 1982; Wang and Maler 1994; Berman and Maler 1999). Granule cell bodies in the EGP stain positive for *Apt*Kv3.3 (not shown), although their projections do not (see Distribution of AptKv3.3 in the apteronotid ELL). Running orthogonal to the parallel fibers are the vertical fibers. Vertical fibers have been proposed to arise from the eurydendroid cells (Wang and Maler 1994; Berman and Maler 1999), which are believed to be cholinergic, and probably provide diffuse modulatory inputs via muscarinic receptors (Maler et al. 1981; Phan and Maler 1983). Dendrites and somata of putative eurydendroid cells stain positive for *Apt*Kv3.3 (Fig. 2c). Finally, Purkinje cells of the CCb stain positive for *Apt*Kv3.3 (Fig. 2d) channels, consistent with the high-threshold currents found in these cells in mammals (Martina et al. 2003; McKay and Turner 2004). This again suggests that much of the electrosensory-related cerebellum is capable of firing at high frequencies correlated with Kv3 channel expression.

Differential properties of dendritic and somatic Kv3 channels

As stated above, a strong localization of *Apt*Kv3.3 can be found in the soma and proximal and distal dendrites of ELL pyramidal cells (Fig. 3a). Further, outside-out patch recordings pulled from either dendrites (Fig. 3b) or somata (Fig. 3d) confirm the presence of channels with a conductance, voltage dependence, and sensitivity to low concentrations of tetraethylammonium (TEA) (Fig. 3c, gray trace), indicative of the Kv3 family (Coetzee et al. 1999; Rashid et al. 2001a). We recently showed that *Apt*Kv3.3 channels can undergo a very fast rate of inactivation in expression systems when the initiation site for transcription is assured by providing a strong Kozak consensus sequence (Fernandez et al. 2003). Nevertheless, these channels prove to display a slow rate of inactivation in both somatic and dendritic regions of pyramidal cells in situ (Rashid et al. 2001a). The reason for differences between *Apt*Kv3.3 in expression systems and *Apt*Kv3 currents in pyramidal cells is unknown, but likely relates to the modulation by potential heteromeric expression with other Kv3 family subunits or unknown post-transcriptional factors.

One of the most studied aspects of the ELL pyramidal cell is a characteristic mode of frequency-dependent burst output (Turner et al. 1994; Lemon and Turner 2000; Doiron et al. 2001, 2003; Noonan et al. 2003; Krahe and Gabbiani 2004). Burst firing in pyramidal cells involves an increasing degree of mismatch between the duration of the dendritic and somatic spikes during repetitive activity. Each somatic spike initiates a back-propagating dendritic spike (Fig. 4a 1, 2). The dendritic spike has a spatial and temporal delay, leading to a difference between the membrane potential in the two compartments. The resulting dendro-somatic flow of current creates a depolarizing afterpotential at the soma that advances the phase of the next spike. This continues until the somatic spike occurs within the refractory period of the dendritic spike, leading to a dendritic spike failure (Fig. 4b) (Lemon and Turner 2000; Noonan et al. 2003; for review see Turner et al. 2002). The threshold for this bursting behavior is dependent on the repetitive discharge at frequencies beyond approximately 100 Hz and is regulated by *Apt*Kv3 K^+ channels. As shown (Fig. 3a–c), both soma and dendrites contain highly TEA-sensitive K^+ conductances. TEA at low concentrations is also known to block other K^+ channels, including members of the Kv1 family and the large conductance calcium-activated K^+ channel (Coetzee et al. 1999). We have shown in both soma (Fig. 4c) and dendrites (Fig. 4d) that α-dendrotoxin (200 nM), a specific Kv1 blocker, has no effect on spike waveforms. Further, the specific large conductance calcium-activated

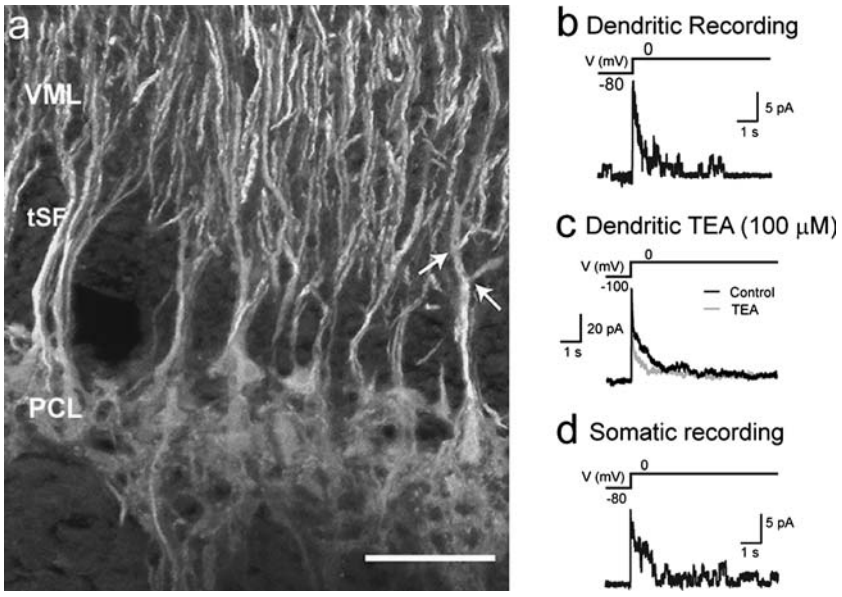

Fig. 3 *Apt*Kv3.3 K^+ channels are highly expressed in ELL pyramidal cells. **a** Immunolabel for *Apt*Kv3.3 K^+ channels reveals an extensive distribution over the entire soma-dendritic axis of pyramidal cells. *Arrows* indicate labeling past primary and secondary branchpoints. *PCL* pyramidal cell layer, *tSF* tractus stratum fibrosum, *VML* ventral molecular layer. *Scale bar* represents 100 μm. **b** Outside-out patch clamp recordings obtained from the proximal apical dendrites reveal a high density of slowly inactivating K^+ channels consistent with Kv3.3 channel kinetics. **c** Low concentrations of TEA block *Apt*Kv3 channels, shown here for a dendritic outside-out macropatch recording. Control trace is in *black*, while TEA application is in *gray*. **d** Somatic outside-out patch clamp reveals a kinetically similar channel expressed in the somata of pyramidal cells. (Data from Rashid et al. 2001b)

K^+ channel blocker iberiotoxin fails to have any noticeable effects on spike waveform (Noonan et al. 2003). In comparison, TEA increases the spike width in both dendrite and soma and abolishes a fast afterhyperpolarization in somatic recordings (Fig. 4c, d, gray traces), suggesting that *Apt*Kv3 K^+ channels play an important role in spike repolarization in both compartments.

Although both soma and dendrite display sensitivity to TEA, the effects on burst output vary between the two compartments. Since bursting depends on a mismatch between the duration of the somatic and dendritic spikes, events that alter spike durations have distinct effects. Focal ejections of TEA to the dendrite fail to have any measurable effect on somatic spike waveform, but widen the dendritic spike, and selectively increase the size of the associated depolarizing afterpotential. By increasing the disparity between somatic and dendritic membrane potentials, burst threshold is reduced (Fig. 3e) and the cell begins bursting almost immediately. In contrast, when the somatic spike is widened by TEA, the disparity between compartments is reduced, leading to a dramatic increase in burst threshold (Fig. 3f). We can, therefore, identify dendritic *Apt*Kv3-related K^+ channels as crucial to the regulation of burst threshold in ELL pyramidal cells by restricting somatic and dendritic spike widths to set the size of the depolarizing afterpotential (Noonan et al. 2003). This potential is required for the parcellation of inputs into bursts coding low-frequency regions of the amplitude modulations or isolated spikes coding for high-frequency regions (Oswald et al. 2004). The potential role for *Apt*Kv3 channels in participating in the spike-to-spike process underlying burst discharge has been reviewed elsewhere (Turner et al. 2002). Instead, the remainder of this review will focus on the role of K^+ channels in determining the high frequencies of spike discharge necessary to promote bursting.

Kinetics of high and low-threshold potassium channels in ELL pyramidal cells

Fast firing cells that express a member of the Kv3 family also typically express low-threshold K^+ channels, often of the Kv1 family (Weiser et al. 1994; Wang et al. 1998; Dodson et al. 2003; Ishikawa et al. 2003; McKay et al. 2005). These low-threshold currents have been suggested as being key to regulating subthreshold excitability to ensure appropriate signal-to-noise ratios (Svirskis et al. 2002), as well as setting the rheobase of spiking (Dodson et al. 2003; Ishikawa et al. 2003). Pyramidal cells of the ELL are no exception, expressing both TEA-sensitive high-threshold channels and TEA-insensitive low-threshold K^+ channels (Fernandez et al. 2005). For the purpose of discussion, we will refer to these two currents as high threshold (IK_{HT}) or low threshold (IK_{LT}). The molecular identity of IK_{LT} is as yet unknown, although the insensitivity of the spike waveform to α-dendrotoxin would suggest they are not comprised of Kv1.1, Kv1.2, or Kv1.6 subunits. We have, therefore, used TEA to separate out the TEA-sensitive IK_{HT} from the

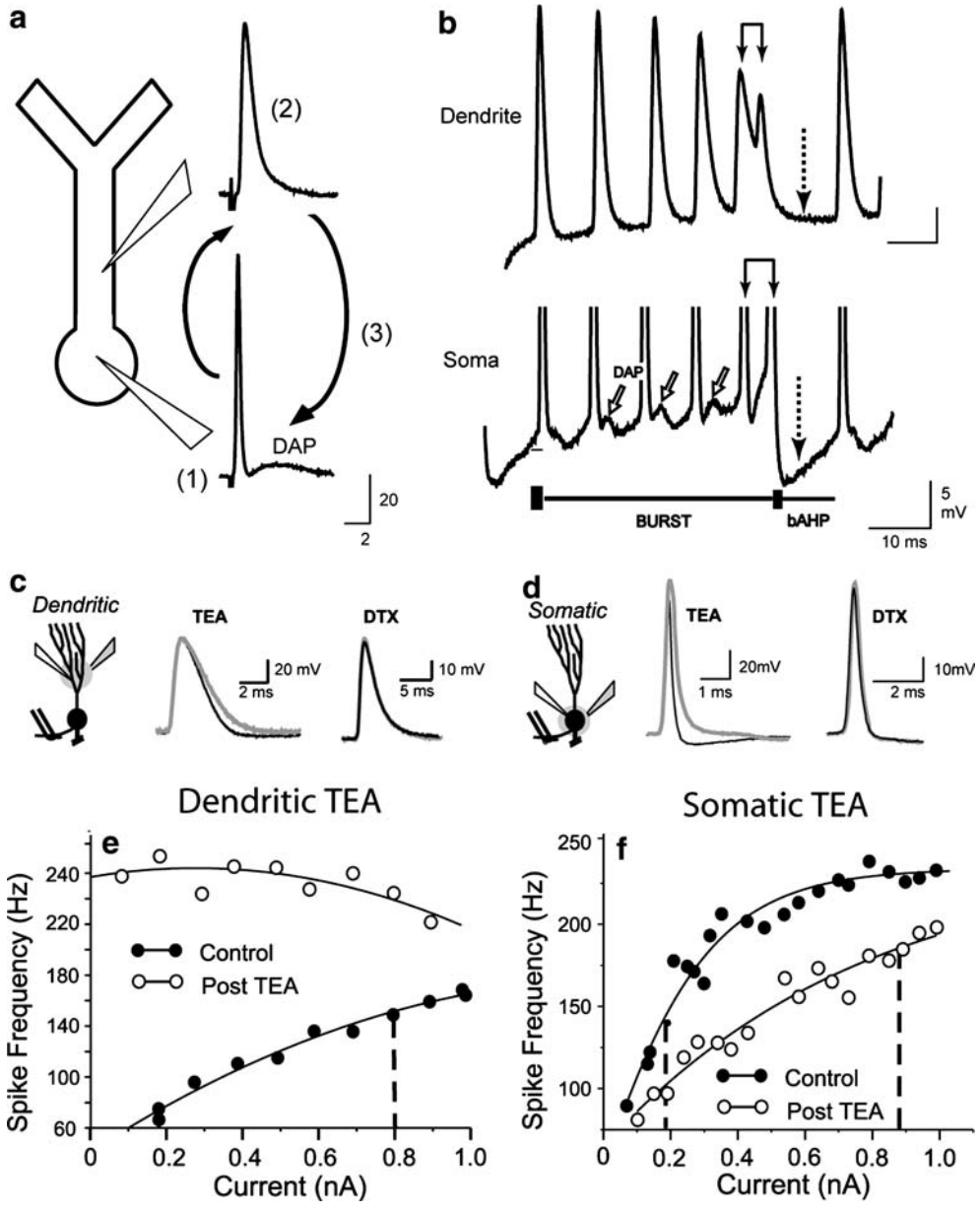

Fig. 4 *Apt*Kv3 K^+ channels regulate burst discharge in ELL pyramidal cells. **a** Schematic diagram of a pyramidal cell soma and apical dendrite depicting Na^+ spike initiation in the somatic region (*1*) and subsequent active backpropagation over approximately 200 μm of an 800 μm dendritic tree (*2*). A relatively long duration dendritic spike compared to the soma leads to return current flow during backpropagation that generates a depolarizing afterpotential (*DAP*) at the soma (*3*). **b** Schematic diagram of events during repetitive discharge that produce a spike burst. Representative traces of single spike bursts from separate dendritic (*top*) and somatic (*bottom*) recordings are shown aligned for illustrative purposes. Dendritic spikes exhibit a frequency-dependent broadening that increases current flow to the soma (*hollow arrows*) to potentiate DAP amplitude. Eventually, a spike doublet is triggered at the soma (*double linked arrows*) with an interspike interval that falls inside the dendritic refractory period. A loss of the dendritic spike removes the depolarization driving the burst (*dashed arrow*), and the cell generates a burst afterhyperpolarization (*bAHP*). **c**, **d** The contribution of TEA-sensitive K^+ channels to spike repolarization and afterpotentials. Schematic diagrams illustrate the placement of recording electrodes and focal pressure ejection of drugs at the level of apical dendrites (**c**) or soma (**d**). *Double wires* indicate position of stimulating electrodes to evoke antidromic spike discharge. Superimposed traces of antidromic dendritic and somatic spike discharge are shown before and after focal ejection of 1 mM TEA or 500 μM dendrotoxin (*DTX*). Control recordings are *thin black traces*, and post-ejection recordings are *thick gray traces*. In both soma and dendrite, TEA widens the spike, while DTX fails to affect the spike waveform. **e**, **f** Dendritic and somatic K^+ channels differentially regulate burst discharge. Representative frequency–current plots of mean spike frequency obtained before and after focal ejection of 1 mM TEA in either the dendritic (**e**) or somatic region (**f**). An initial frequency–current plot indicates a gradual increase in spike frequency that shifts to a burst output at 0.8 nA current injection (**e**, *dashed line*). Focal dendritic TEA ejection increases somatic spike frequency and lowers the threshold for burst discharge to approximately 0.1 nA (**e**). A separate somatic recording indicating that focal ejections of TEA in the cell body layer lowers spike frequency and raises burst threshold from 0.2 to 0.9 nA (**f**). (Data from Noonan et al. 2003)

low-threshold TEA-insensitive IK_{LT}. Because of this methodology we cannot distinguish between the subunits making up the TEA-sensitive current, although their kinetics and pharmacology would suggest members of the *Apt*Kv3 family.

The IK_{HT} component of the somatic K^+ current recorded with whole cell voltage clamp (Fig. 5a) is fast activating (τ_{act} varying between 0.5 and 2 ms) (Fig. 5d). Although some inactivation can be seen in longer voltage pulses (F. Fernandez, unpublished observation), it is consistently non-inactivating over a 100 ms time scale. It displays a high voltage for half-activation ($V_{1/2}$) of −15 mV. Although this is lower than the $V_{1/2}$ reported for both mammalian and apteronotid Kv3 channels in expression systems (Critz et al. 1993; Kanemasa et al. 1995; Wang et al. 1998; Fernandez et al. 2005), it is similar to the currents commonly found in in vitro neural preparations (Shibata et al. 1999; Baranauskas et al. 2003; Martina et al. 2003; McKay and Turner 2004).

Although operating on a similar time scale for activation (Fig. 5b), IK_{LT} shows a slower deactivation at mid-range voltages (Fig. 5d) than IK_{HT}. IK_{LT} is also a non-inactivating current, which shows a significantly lower $V_{1/2}$ (−37 mV) than IK_{HT}. This makes IK_{LT} an ideal candidate to regulate subthreshold excitability and improve signal-to-noise ratio (Svirskis et al. 2002; Dodson et al. 2003) or to detect slopes of inputs to the cell (Ferragamo and Oertel 2002).

Interaction between high and low-threshold K^+ currents

Traditionally, the expression of IK_{HT} was thought to increase the ability for neurons to fire at high frequencies by creating a fast afterhyperpolarization, allowing more recovery of Na^+ current from inactivation after each spike. We have recently shown that there is an additional element involved in IK_{HT} contribution to high-frequency firing in ELL pyramidal cells. In particular, we have demonstrated that the relative contributions of IK_{HT} and IK_{LT} show a frequency dependence, which can be seen in the frequency–current plots and in the currents themselves in both voltage clamp mode and models based on the recorded kinetics described above.

In order to examine the behavior of the current during repetitive firing, we can use recorded trains of spikes played back to pyramidal cells recorded in voltage clamp mode. Dissecting the current with TEA uncovers frequency-dependent and separate contributions by IK_{HT} and IK_{LT} to spike discharge. At low frequencies, both IK_{HT} and IK_{LT} are activated by each spike and are

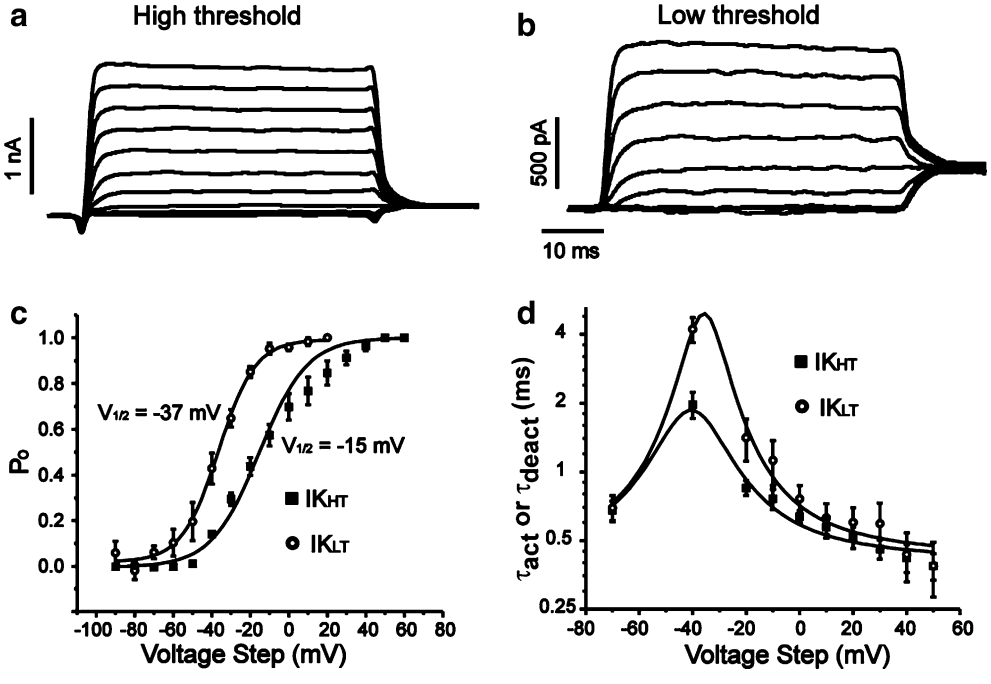

Fig. 5 Kinetics of K^+ currents in whole cell recordings from ELL pyramidal cells. **a** Representative example of the high-threshold, TEA-sensitive current (IK_{HT}) evoked by square voltage steps from −70 to 40 mV for IK_{HT}, with 10 mV steps. **b** Low-threshold, TEA-insensitive current (IK_{LT}) evoked by voltage steps from −70 to 10 mV in 10 mV increments. **c** Open probability (P_o) plotted as a function of voltage for IK_{HT} and IK_{LT}. The mean $V_{1/2}$ of activation for IK_{HT} and IK_{LT} was -15.3 ± 0.6 mV and -36.5 ± 1.2 mV, respectively. **d** Time constants of activation (τ_{act}) and deactivation (τ_{deact}) plotted as a function of voltage. Contrary to a two-state Hodgkin–Huxley model, the deactivation time constants for IK_{HT} are relatively slow compared to activation, suggesting a more complicated gating scheme. Time course of activation and deactivation are fit with a fourth power and standard exponential function, respectively. The relationship between time constant and voltage is fit with Lorentzian functions. (Data from Fernandez et al. 2005)

capable of completely deactivating over the time course of the interspike interval (Fig. 6a). In contrast, at high frequencies IK_{LT} begins to accumulate, while IK_{HT} never builds up, regardless of the frequency (Fig. 6b).

When these currents are placed in a firing model of the ELL pyramidal cell along with a Na^+ current and a leak conductance (for details, see Fernandez et al. 2005), a similar frequency dependence can be seen. As found in pyramidal cells, at low discharge frequencies both currents are able to completely deactivate during the interspike interval. At high frequencies, IK_{LT} in the firing model accumulates between spikes and creates a shift in baseline current, but only if IK_{HT} is absent. If IK_{HT} is present, both currents are able to deactivate during the interspike interval (Fig. 6c). When the model currents are replayed the model spike waveforms as voltage clamp commands, these currents display the same behavior as the currents in pyramidal cells. At high, but not low frequencies, IK_{LT} accumulates while IK_{HT} does not (Fig. 6d). This accumulation of IK_{LT} leads to a dampening of excitability at high frequencies in both the pyramidal cell and the firing model.

The role for IK_{HT} in regulating pyramidal cell discharge becomes apparent upon the application of TEA, when the firing output is selectively dampened at high frequencies, but not at low frequencies (Fig. 6e). This dampening is correlated with many features consistent with an accumulation of Na^+ channel inactivation during repetitive discharge, including decreases in the rate of rise and loss of spike height (Fernandez et al. 2005). Earlier reports suggested that IK_{HT} is expressed to prevent these effects on Na^+ current during high frequencies of discharge (Erisir et al. 1999). However, by manipulating the responsible variables in a firing model, we find that inactivation of Na^+ current is not the sole factor preventing the system from firing at high frequencies. In the firing model without IK_{HT} (Fig. 6f, no IK_{HT}, circle with a dot), we have imposed a reset of the Na^+ inactivation variable h to a value enabling repetitive firing. This tests whether the sole effect of IK_{HT} is to deinactivate Na^+ channels during high-frequency discharge. In fact, this manipulation is insufficient to recover the gain of the frequency–current relationship observed before removing IK_{HT} (Fig. 6f, h reset, inverted filled triangle). Since IK_{LT} accumulated in the firing model, we have tested whether its accumulation significantly dampens firing. Preventing the accumulation of IK_{LT} activation variable n by resetting it between spikes also fails to fully recover the firing profile (Fig. 6f, n reset, triangle with a dot). To fully recover the normal frequency–current plot we found that both variables must be reset (Fig. 6f, with IK_{HT}, filled square), showing that both Na^+ channel inactivation and an accumulation of IK_{LT} are responsible for the reduced ability to fire at high frequencies. This suggests that one of the roles of IK_{HT} is to actually reduce the contribution of IK_{LT} at high frequencies, preventing its dampening effects, while still allowing it to regulate the subthreshold excitability. Given the regularity with which high and low-threshold K^+ currents are co-expressed, this interplay between K^+ conductances may be common in high-frequency firing cells. These data further emphasize that interactions between K^+ channels can regulate fine details of firing beyond those predicted by their independent effects. As various K^+ channels have been suggested to have specific roles in regulating neuronal output, it will be informative to more carefully examine their interactions to fully understand the complex behaviors they can contribute to.

Discussion

As the ELL performs key computations in signal processing that require high temporal acuity, it is consistent that many of the cells involved in either relaying or modifying ELL output express at least one member of the Kv3 channel family (Rashid et al. 2001a). These channels are widely associated with high-frequency firing in systems where exact timing is important (Perney et al. 1992; Brew and Forsythe 1995; Trussell 1997; Gan and Kaczmarek 1998; Wang et al. 1998; Erisir et al. 1999; Shibata et al. 1999; Parameshwaran et al. 2001; Ishikawa et al. 2003). The electrosensory system is one example of such a system, with an ability to discriminate extremely fine differences in timing (Carr et al. 1986; Carr and Maler 1986).

*Apt*Kv3.3 channels are highly expressed along the soma-dendritic axis of ELL pyramidal cells (Rashid et al. 2001b), the primary output cell for much of the electrosensory information. A dendritic distribution of *Apt*Kv3.3 K^+ channels is novel, because much of the labeling reported for other members of the Kv3 family (Kv3.1, 3.2, and 3.4) in other cells has been restricted to somata and axons (Weiser et al. 1995). Further, many of the dendritic K^+ channels previously described have low-threshold members of the Kv4 family or calcium-activated K^+ conductances (Hoffman et al. 1997; Cai et al. 2004). Our studies have demonstrated an important role for *Apt*Kv3 currents in repolarizing both somatic and backpropagating dendritic spikes (Rashid et al. 2001b; Noonan et al. 2003). Further, somatic and dendritic *Apt*Kv3.3 channels are able to differentially regulate burst output, allowing separate effects for the same channel in distinct compartments of a single cell (Noonan et al. 2003). These bursts are of significant computational importance for the coding of inputs (Gabbiani et al. 1996; Krahe and Gabbiani 2004), and the dendritic contribution to spike output plays an important role in this phenomenon. In particular, bursts of activity have been suggested to code preferentially for low-frequency components of amplitude modulations, while high-frequency components are coded by isolated spikes. This division is critically dependent on depolarizing afterpotentials (Oswald et al. 2004) that are regulated by Kv3 channels (Noonan et al. 2003).

A dendritic distribution of Kv3 channels was recently reported for mammalian cerebellar Purkinje cells, a

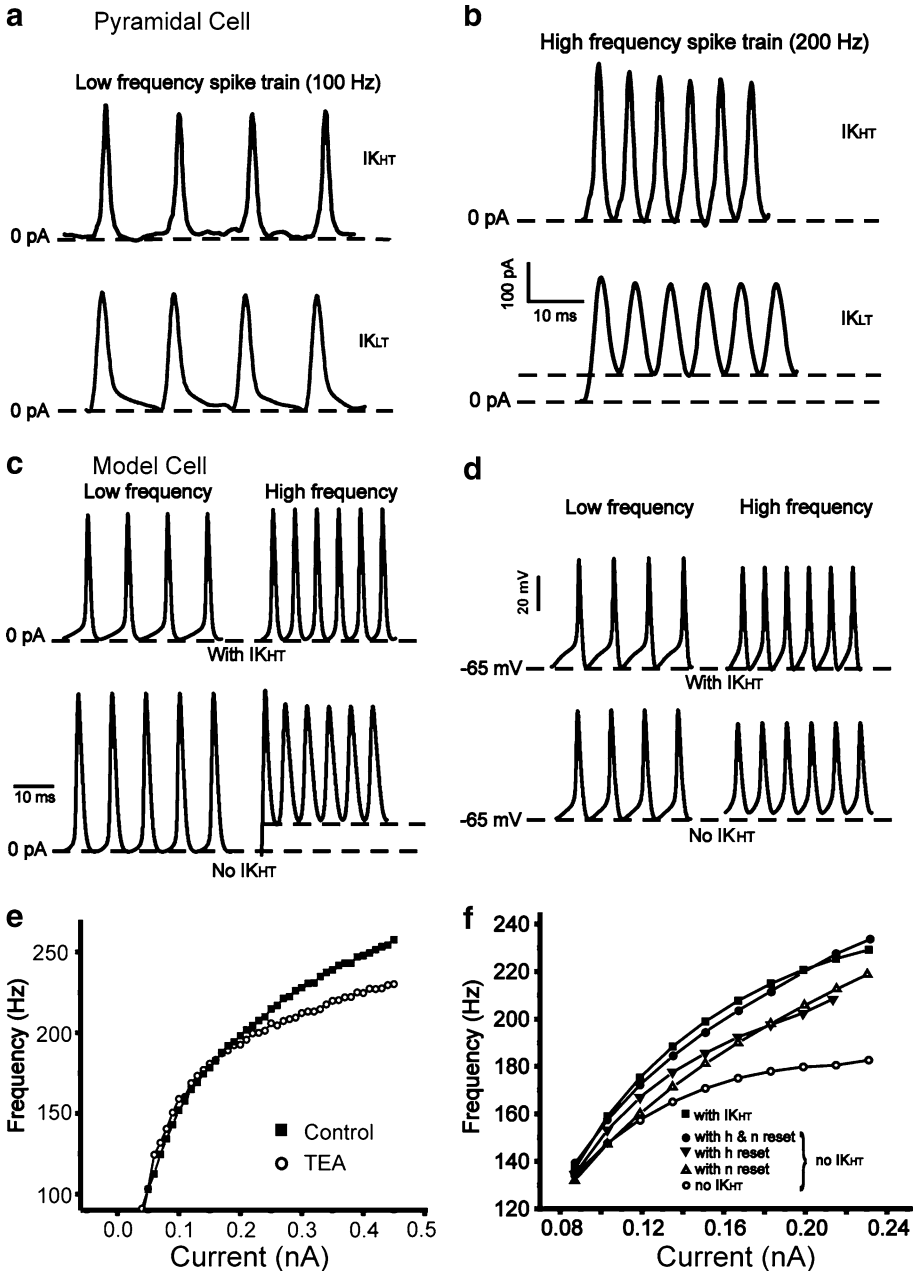

Fig. 6 Low-threshold K^+ current shows a frequency-dependent accumulation during the interspike interval, increasing the refractory period of the neuron. **a** Whole cell K^+ currents recorded from pyramidal cells (isolated after TEA application) evoked using spike waveforms. Spike waveforms consisted of spikes with interspike interval (*ISI*) voltages of −60 mV, a half-width of 1 ms, and a spike height of 70 mV (−70 to 0 mV). Using 100 Hz spike trains, both IK_{HT} and IK_{LT} show little or no current during the ISI. **b** At 200 Hz, IK_{HT} continues to show no current during the interspike interval, but now IK_{LT} shows an increase in baseline current (*lower trace*). **c** IK_{LT} produced from the spikes shown in **d.** The change in afterhyperpolarization size and the general increase in interspike voltage at high frequencies without IK_{HT} (**d**, *bottom right*) lead to an increase in IK_{LT} during the ISI in the high-frequency condition. This replicates the pyramidal cell data (**a**, **b**). **d** Spike waveforms at low and high firing frequencies. Waveforms taken from a firing model incorporating the K^+ currents recorded in the pyramidal cell are shown at low and high firing frequencies in the presence or absence of IK_{HT}. Note that without IK_{HT}, the peak negative voltage during low-frequency firing reaches −65 mV (*bottom, left*), while at high frequencies this value rises well above −60 mV (*bottom, right*). **e** Comparison of the frequency–current relationship generated by the pyramidal cell either with IK_{HT} intact (control, *filled square*) or blocked by TEA (*circle with a dot*). Without IK_{HT}, the cell loses the ability to fire at high frequencies. **f** Comparison of the frequency–current relation generated from the model after between-spike resetting of either the sodium inactivation variable between spikes (h reset, *inverted filled triangle*) or the K^+ activation variable (n reset, *triangle with a dot*). Neither manipulation fully restores the frequency–current plot to the control conditions (*filled circle*), but each provides partial recovery compared to the no-IK_{HT} condition (*circle with a dot*). Resetting both the n and h reset generates a frequency–current relation nearly identical to that with IK_{HT}. (Data from Fernandez et al. 2005)

result consistent with our demonstration of *Apt*Kv3.3 immunolabel in apertonotid cerebellum (Martina et al. 1998; Rashid et al. 2001a; McKay and Turner 2004). We have also shown that dendritic Kv3 channels in rat Purkinje cells have an important role in repolarizing both Na^+ as well as the large amplitude Ca^{2+} spikes inherent to these cells (McKay and Turner 2004). By restraining the amplitude and duration of Ca^{2+} spikes, Kv3 channels are able to prevent a rapid inactivation of somatic Na^+ spikes and thus the final output of the cell. The properties of cerebellar Purkinje cells in weakly electric fish are also beginning to be characterized (Han and Bell 2003). The similarity of spike discharge properties in mormyrid cerebellar Purkinje cells to those established in mammals suggests that Kv3 channels will serve a similar purpose across a wide range of species.

We have concentrated here on the K^+ currents underlying spike discharge in the ELL, although the currents underlying electrosensory outputs have also been studied. Of particular note, neurons of the pacemaker nucleus of *Apteronotus* are able to fire at extremely high frequencies (>1 kHz). The output of these extremely fast firing cells is TEA insensitive, suggesting that a non-Kv3 channel is responsible for spike repolarization. Specifically, the molecular identity of the pacemaker nucleus repolarizer has been suggested to be Kv1.4 or 1.5 (Smith and Zakon 2000). This is consistent with the small amplitude (~30 mV) of pacemaker nucleus spikes (Smith and Zakon 2000), which would be unlikely to activate high-threshold Kv3 currents, but would activate lower threshold Kv1 currents. The K^+ currents found in electrocytes of the electric organ have also been characterized and shown to co-regulate their kinetics to match changes in Na^+ kinetics to scale electrocyte firing rates in the weakly electric fish of the genus *Sternopygus*. The K^+ current in electrocytes is fast activating and deactivating, with a fairly high V_{onset} of approximately −40 mV, suggesting it may be a high-threshold channel (McAnelly and Zakon 2000). Because spherical cells in the ELL can code phase information even when EOD frequency is high (Carr et al. 1986), they may use a similar mechanism. This would be consistent with our failure to find strong immunolabel for *Apt*Kv3.3 in spherical cell bodies or proximal axons. It would thus appear that other K^+ channel subtypes also have the capacity to act as a fast repolarizing current, a role that is often automatically attributed to Kv3 channels.

Although the recorded $V_{1/2}$ of the Kv3 current we describe is significantly lower than those recorded in expression systems (Critz et al. 1993; Kanemasa et al. 1995; Fernandez et al. 2003), it is similar to the currents commonly recorded in neurons in vitro (Shibata et al. 1999; Baranauskas et al. 2003; McKay and Turner 2004). Numerous intracellular factors have been shown to be capable of modulating Kv3 K^+ channels (Macica and Kaczmarek 2001; Lewis et al. 2004; von Hehn et al. 2004), and changes have been reported due to heteromerization between members of the Kv3 family (Baranauskas et al. 2003). We do not yet know what is responsible for differences between *Apt*Kv3 channels in expression systems and the pyramidal cell, but our results reveal that these channels are capable of exhibiting a wide range of kinetic and inactivation properties. Regulation of these parameters by intracellular factors could then greatly increase the relative contribution of *Apt*Kv3.3 channels to different processing requirements, either in other cells in the ELL or in pyramidal cells across the multiple ELL maps.

Extensive work on Kv3 K^+ channels in mammalian cells has led to an understanding of their role in preventing cumulative Na^+ channel inactivation at high frequencies of discharge (Erisir et al. 1999). This function has been identified primarily in terms of their ability to prevent a rapid failure of Na^+ spike discharge. Our work supports this interpretation, but extends the analysis to consider how Kv3 channels can regulate Na^+ channel availability to affect the input–output relation at sustainable spike frequencies. Specifically, we recently identified an important and surprising aspect of how Kv3 channels interact with other K^+ currents to invoke a frequency-dependent contribution to input–output gain. As in all other high-frequency firing cells, *Apt*Kv3 channels are expressed along with a low-threshold delayed rectifier with kinetics suggestive of the Kv1 family. Previous experiments with α-dendrotoxin suggest it is not Kv1.1, Kv1.2, or Kv1.6, although the latter is commonly co-expressed with Kv3s in the neocortex (Toledo-Rodriguez et al. 2004), while Kv1.1 and Kv1.2 channels are co-expressed with Kv3 in the auditory system (Dodson et al. 2002, 2003; Barnes-Davies et al. 2004). Low-threshold K^+ channels can regulate the threshold for spike discharge, but we show that they can also decrease the excitability at higher frequencies of discharge.

Our results indicate that this previously unrecognized cumulative activation of IK_{LT} is a key contributor to the depression of firing at high frequencies. Moreover, co-expression of Kv3 current counteracts the accumulation of IK_{LT}, providing a selective control of IK_{LT} in the high-frequency range without affecting its determination of spike threshold. This leads to a frequency-dependent increase in gain in pyramidal cells that is reflected in a selective TEA sensitivity of several spike parameters, including the rate of spike repolarization and afterhyperpolarization (Fernandez et al. 2005). Although some of these changes can be traced to a cumulative increase in Na^+ channel inactivation, we have shown how the effects of Kv3 channels on IK_{LT} are at least as important in determining its ability to maintain high frequencies of discharge. This interaction allows a cell to retain the advantages of IK_{LT} in regulating spike threshold without it interfering with high-frequency output.

Acknowledgements We gratefully acknowledge E. Morales and L. Noonan for earlier work on Kv3 channels and the expert technical assistance of M. Kruskic and M. LaChance. The work

reviewed here was supported by a CIHR grant and CIHR Group Grant (RWT, RD), a CIHR Doctoral Studentship (FRF), Alberta Provincial Graduate Scholarships (FRF, WHM), and an AHFMR Scientist Award (RWT).

References

Baranauskas G, Tkatch T, Nagata K, Yeh JZ, Surmeier DJ (2003) Kv3.4 subunits enhance the repolarizing efficiency of Kv3.1 channels in fast-spiking neurons. Nat Neurosci 6:258–266

Barnes-Davies M, Barker MC, Osmani F and Forsythe ID (2004) Kv1 currents mediate a gradient of principal neuron excitability across the tonotopic axis in the rat lateral superior olive. Eur J Neurosci 19:25–33

Bastian J (1986a) Gain control in the electrosensory system mediated by descending inputs to the electrosensory lateral line lobe. J Neurosci 6:553–562

Bastian J (1986b) Gain control in the electrosensory system: a role for the descending projections to the electrosensory lateral line lobe. J Comp Physiol A 158:505–515

Bastian J, Courtright J (1991) Morphological correlates of pyramidal cell adaptation rate in the electrosensory lateral line lobe of weakly electric fish. J Comp Physiol A 168:393–407

Bastian J, Nguyenkim J (2001) Dendritic modulation of burst-like firing in sensory neurons. J Neurophysiol 85:10–22

Bastian J, Courtright J, Crawford J (1993) Commissural neurons of the electrosensory lateral line lobe of *Apteronotus leptorhynchus*: morphological and physiological characteristics. J Comp Physiol A 173:257–274

Bastian J, Chacron MJ, Maler L (2004) Plastic and nonplastic pyramidal cells perform unique roles in a network capable of adaptive redundancy reduction. Neuron 41:767–779

Berman NJ, Maler L (1998) Interaction of GABAB-mediated inhibition with voltage-gated currents of pyramidal cells: computational mechanism of a sensory searchlight. J Neurophysiol 80:3197–3213

Berman NJ, Maler L (1999) Neural architecture of the electrosensory lateral line lobe: adaptations for coincidence detection, a sensory searchlight and frequency-dependent adaptive filtering. J Exp Biol 202:1243–1253

Brew HM, Forsythe ID (1995) Two voltage-dependent K+ conductances with complementary functions in postsynaptic integration at a central auditory synapse. J Neurosci 15:8011–8022

Cai X, Liang CW, Muralidharan S, Kao JP, Tang CM, Thompson SM (2004) Unique roles of SK and Kv4.2 potassium channels in dendritic integration. Neuron 44:351–364

Carr CE, Maler L (1986) Electroreception in gymnotiform fish. In: Bullock TH, Heiligenberg W (eds) Electroreception. Wiley, New York, pp 319–373

Carr CE, Heiligenberg W, Rose GJ (1986) A time-comparison circuit in the electric fish midbrain. I. Behavior and physiology. J Neurosci 6:107–119

Chandy KG, Gutman GA (1993) Nomenclature for mammalian potassium channel genes. Trends Pharmacol Sci 14:434

Coetzee WA, Amarillo Y, Chiu J, Chow A, Lau D, McCormack T, Moreno H, Nadal MS, Ozaita A, Pountney D, Saganich M, Vega-Saenz de Miera E, Rudy B (1999) Molecular diversity of K^+ channels. Ann N Y Acad Sci 868:233–285

Critz SD, Wible BA, Lopez HS, Brown AM (1993) Stable expression and regulation of a rat brain K^+ channel. J Neurochem 60:1175–1178

Dodson PD, Barker MC, Forsythe ID (2002) Two heteromeric Kv1 potassium channels differentially regulate action potential firing. J Neurosci 22:6953–6961

Dodson PD, Billups B, Rusznak Z, Szucs G, Barker MC, Forsythe ID (2003) Presynaptic rat Kv1.2 channels suppress synaptic terminal hyperexcitability following action potential invasion. J Physiol 550:27–33

Doiron B, Longtin A, Turner RW, Maler L (2001) Model of gamma frequency burst discharge generated by conditional backpropagation. J Neurophysiol 86:1523–1545

Doiron B, Noonan L, Lemon N, Turner RW (2003) Persistent Na^+ current modifies burst discharge by regulating conditional backpropagation of dendritic spikes. J Neurophysiol 89:324–337

Dunlap KD (2002) Hormonal and body size correlates of electrocommunication behavior during dyadic interactions in a weakly electric fish, *Apteronotus leptorhynchus*. Horm Behav 41:187–194

Dunlap KD, Larkins-Ford J (2003) Diversity in the structure of electrocommunication signals within a genus of electric fish, *Apteronotus*. J Comp Physiol A 189:153–161

Dunlap KD, Oliveri LM (2002) Retreat site selection and social organization in captive electric fish, *Apteronotus leptorhynchus*. J Comp Physiol A 188:469–477

Erisir A, Lau D, Rudy B, Leonard CS (1999) Function of specific K^+ channels in sustained high-frequency firing of fast-spiking neocortical interneurons. J Neurophysiol 82:2476–2489

Fernandez FR, Morales E, Rashid AJ, Dunn RJ, Turner RW (2003) Inactivation of Kv3.3 potassium channels in heterologous expression systems. J Biol Chem 278:40890–40898

Fernandez FR, Mehaffey WH, Molineux ML, Turner RW (2005) High-threshold K^+ current increases gain by offsetting a frequency-dependent increase in low-threshold K^+ current. J Neurosci 25:363–371

Ferragamo MJ, Oertel D (2002) Octopus cells of the mammalian ventral cochlear nucleus sense the rate of depolarization. J Neurophysiol 87:2262–2270

Gabbiani F, Metzner W, Wessel R, Koch C (1996) From stimulus encoding to feature extraction in weakly electric fish. Nature 384:564–567

Gan L, Kaczmarek LK (1998) When, where, and how much? Expression of the Kv3.1 potassium channel in high-frequency firing neurons. J Neurobiol 37:69–79

Han VZ, Bell CC (2003) Physiology of cells in the central lobes of the mormyrid cerebellum. J Neurosci 23:11147–11157

Heiligenberg W (1986) Jamming avoidance responses: model systems for neuroethology. In: Bullock TH, Heiligenberg W (eds) Electroreception. Wiley, New York, pp 613–649

Heiligenberg W (1991) Neural nets in electric fish. MIT Press, Cambridge

von Hehn CA, Bhattacharjee A, Kaczmarek LK (2004) Loss of Kv3.1 tonotopicity and alterations in cAMP response element-binding protein signaling in central auditory neurons of hearing impaired mice. J Neurosci 24:1936–1940

Hodgkin AL, Huxley AF (1952) Movement of sodium and potassium ions during nervous activity. Cold Spring Harb Symp Quant Biol 17:43–52

Hoffman DA, Magee JC, Colbert CM, Johnston D (1997) K^+ channel regulation of signal propagation in dendrites of hippocampal pyramidal neurons. Nature 387:869–875

Ishikawa T, Nakamura Y, Saitoh N, Li WB, Iwasaki S, Takahashi T (2003) Distinct roles of Kv1 and Kv3 potassium channels at the calyx of held presynaptic terminal. J Neurosci 23:10445–10453

Kanemasa T, Gan L, Perney TM, Wang LY, Kaczmarek LK (1995) Electrophysiological and pharmacological characterization of a mammalian Shaw channel expressed in NIH 3T3 fibroblasts. J Neurophysiol 74:207–217

Krahe R, Gabbiani F (2004) Burst firing in sensory systems. Nat Rev Neurosci 5:13–23

Lannoo MJ, Maler L, Tinner B (1989) Ganglion cell arrangement and axonal trajectories in the anterior lateral line nerve of the weakly electric fish *Apteronotus leptorhynchus* (Gymnotiformes). J Comp Neurol 280:331–342

Lee TE, Philipson LH, Nelson DJ (1996) N-type inactivation in the mammalian Shaker K^+ channel Kv1.4. J Membr Biol 151:225–235

Lemon N, Turner RW (2000) Conditional spike backpropagation generates burst discharge in a sensory neuron. J Neurophysiol 84:1519–1530

Lewis A, McCrossan ZA, Abbott GW (2004) MinK, MiRP1, and MiRP2 diversify Kv3.1 and Kv3.2 potassium channel gating. J Biol Chem 279:7884–7892

Lien CC, Jonas P (2003) Kv3 potassium conductance is necessary and kinetically optimized for high-frequency action potential generation in hippocampal interneurons. J Neurosci 23:2058–2068

Macica CM, Kaczmarek LK (2001) Casein kinase 2 determines the voltage dependence of the Kv3.1 channel in auditory neurons and transfected cells. J Neurosci 21:1160–1168

MacIver MA, Sharabash NM, Nelson ME (2001) Prey-capture behavior in gymnotid electric fish: motion analysis and effects of water conductivity. J Exp Biol 204:543–557

Maler L (1979) The posterior lateral line lobe of certain gymnotoid fish: quantitative light microscopy. J Comp Neurol 183:323–363

Maler L, Mugnaini E (1994) Correlating gamma-aminobutyricacidergic circuits and sensory function in the electrosensory lateral line lobe of a gymnotiform fish. J Comp Neurol 345:224–252

Maler L, Sas EK, Rogers J (1981) The cytology of the posterior lateral line lobe of high-frequency weakly electric fish (Gymnotidae): dendritic differentiation and synaptic specificity in a simple cortex. J Comp Neurol 195:87–139

Maler L, Sas E, Carr CE, Matsubara J (1982) Efferent projections of the posterior lateral line lobe in gymnotiform fish. J Comp Neurol 211:154–164

Martina M, Schultz JH, Ehmke H, Monyer H, Jonas P (1998) Functional and molecular differences between voltage-gated K^+ channels of fast-spiking interneurons and pyramidal neurons of rat hippocampus. J Neurosci 18:8111–8125

Martina M, Yao GL, Bean BP (2003) Properties and functional role of voltage-dependent potassium channels in dendrites of rat cerebellar Purkinje neurons. J Neurosci 23:5698–5707

McAnelly ML, Zakon HH (2000) Coregulation of voltage-dependent kinetics of Na^+ and K^+ currents in electric organ. J Neurosci 20:3408–3414

McKay BE, Turner RW (2004) Kv3 K^+ channels enable burst output in rat cerebellar Purkinje cells. Eur J Neurosci 20:729–739

McKay BE, Molineux ML, Mehaffey WH, Turner RW (2005) Kv1 K^+ channels control Purkinje cell output to facilitate postsynaptic rebound discharge in deep cerebellar neurons. J Neurosci 25:1481–1492

Mehaffey WH, Doiron B, Maler L, Turner RW (2005) Deterministic multiplicative gain control with active dendrites. J Neurosci 25:9968–9977

Nelson ME, MacIver MA, Coombs S (2002) Modeling electrosensory and mechanosensory images during the predatory behavior of weakly electric fish. Brain Behav Evol 59:199–210

Noonan L, Doiron B, Laing C, Longtin A, Turner RW (2003) A dynamic dendritic refractory period regulates burst discharge in the electrosensory lobe of weakly electric fish. J Neurosci 23:1524–1534

Oswald AM, Chacron MJ, Doiron B, Bastian J, Maler L (2004) Parallel processing of sensory input by bursts and isolated spikes. J Neurosci 24:4351–4362

Parameshwaran S, Carr CE, Perney TM (2001) Expression of the Kv3.1 potassium channel in the avian auditory brainstem. J Neurosci 21:485–494

Perney TM, Marshall J, Martin KA, Hockfield S, Kaczmarek LK (1992) Expression of the mRNAs for the Kv3.1 potassium channel gene in the adult and developing rat brain. J Neurophysiol 68:756–766

Phan M, Maler L (1983) Distribution of muscarinic receptors in the caudal cerebellum and electrosensory lateral line lobe of gymnotiform fish. Neurosci Lett 42:137–143

Rashid AJ, Dunn RJ (1998) Sequence diversity of voltage-gated potassium channels in an electric fish. Mol Brain Res 54:101–107

Rashid AJ, Dunn RJ, Turner RW (2001a) A prominent soma–dendritic distribution of Kv3.3 K^+ channels in electrosensory and cerebellar neurons. J Comp Neurol 441:234–247

Rashid AJ, Morales E, Turner RW, Dunn RJ (2001b) The contribution of dendritic Kv3 K^+ channels to burst threshold in a sensory neuron. J Neurosci 21:125–135

Rudy B, McBain CJ (2001) Kv3 channels: voltage-gated K^+ channels designed for high-frequency repetitive firing. Trends Neurosci 24:517–526

Shibata R, Wakazono Y, Nakahira K, Trimmer JS, Ikenaka K (1999) Expression of Kv3.1 and Kv4.2 genes in developing cerebellar granule cells. Dev Neurosci 21:87–93

Smith GT, Zakon HH (2000) Pharmacological characterization of ionic currents that regulate the pacemaker rhythm in a weakly electric fish. J Neurobiol 42:270–286

Svirskis G, Kotak V, Sanes DH, Rinzel J (2002) Enhancement of signal-to-noise ratio and phase locking for small inputs by a low-threshold outward current in auditory neurons. J Neurosci 22:11019–11025

Tharani Y, Thurlow GA, Turner RW (1996) Distribution of 4-conotoxin GVIA binding sites in teleost cerebellar and electrosensory neurons. J Comp Neurol 364:456–472

Toledo-Rodriguez M, Blumenfeld B, Wu C, Luo J, Attali B, Goodman P, Markram H (2004) Correlation maps allow neuronal electrical properties to be predicted from single-cell gene expression profiles in rat neocortex. Cereb Cortex 14:1310–1327

Trussell LO (1997) Cellular mechanisms for preservation of timing in central auditory pathways. Curr Opin Neurobiol 7:487–492

Turner RW, Moroz LL (1995) Localization of nicotinamide adenine dinucleotide phosphate-diaphorase activity in electrosensory and electromotor systems of a gymnotiform teleost, *Apteronotus leptorhynchus*. J Comp Neurol 356:261–274

Turner RW, Maler L, Deerinck T, Levinson SR, Ellisman MH (1994) TTX-sensitive dendritic sodium channels underlie oscillatory discharge in a vertebrate sensory neuron. J Neurosci 14:6453–6471

Turner RW, Lemon N, Doiron B, Rashid AJ, Morales E, Longtin A, Maler L, Dunn RJ (2002) Oscillatory burst discharge generated through conditional backpropagation of dendritic spikes. J Physiol (Paris) 96:517–530

Wang D, Maler L (1994) The immunocytochemical localization of glutamate in the electrosensory system of the gymnotiform fish, *Apteronotus leptorhynchus*. Brain Res 653:215–222

Wang LY, Gan L, Forsythe ID, Kaczmarek LK (1998) Contribution of the Kv3.1 potassium channel to high-frequency firing in mouse auditory neurones. J Physiol (Lond) 509:183–194

Weiser M, Vega-Saenz de Miera E, Kentros C, Moreno H, Franzen L, Hillman D, Baker H, Rudy B (1994) Differential expression of Shaw-related K^+ channels in the rat central nervous system. J Neurosci 14:949–972

Weiser M, Bueno E, Sekirnjak C, Martone ME, Baker H, Hillman D, Chen S, Thornhill W, Ellisman M, Rudy B (1995) The potassium channel subunit KV3.1b is localized to somatic and axonal membranes of specific populations of CNS neurons. J Neurosci 15:4298–4314

Zakon H, Oestreich J, Tallarovic S, Triefenbach F (2002) EOD modulations of brown ghost electric fish: JARs, chirps, rises, and dips. J Physiol (Paris) 96:451–458